Light Shaping with Holography, GPC and Holo-GPC

Banas, Andrew; Glückstad, Jesper

Published in:
Optical Data Processing and Storage

Link to article, DOI:
10.1515/odps-2017-0004

Publication date:
2017

Document Version
Publisher's PDF, also known as Version of record

Review Article **Open Access**

Andrew Bañas and Jesper Glückstad*

Light Shaping with Holography, GPC and Holo-GPC

DOI 10.1515/odps-2017-0004
Received February 13, 2017; revised April 9, 2017; accepted May 1, 2017

Abstract: Light shaping techniques based on phase-only modulation offer multiple advantages over amplitude modulation. This review examines and compares the merits of two phase modulation techniques; phase-only computer generated holography and Generalized Phase Contrast (GPC). Both techniques are briefly presented while recent developments in GPC will also be covered. Furthermore, novel hybrid schemes that inherit merits from both holography and GPC are also covered. In particular, our most recent technique coined "Holo-GPC" will be discussed in addition to earlier hybrid techniques. We will discuss how Holo-GPC utilizes the simplicity of GPC in forming well-defined speckle-free shapes and the versatility of holography in distributing these shaped beams over an extended 3D volume. To conclude, we cite applications where the combined strengths of the two photon-efficient phase-only light shaping techniques open new possibilities.

Keywords: Generalized Phase Contrast; Holography; Holo-GPC; Laser beam shaping; Fourier optics; Spatial light modulators; Phase-only modulation

1 Introduction: Efficient phase-only light shaping

Laser beam shaping has paved the way for many studies and applications and can be considered as a key enabling tool. Beyond display applications and consumer related areas such as entertainment, dynamic laser distributions can serve as a generic technology for spatially controlled light-matter interaction that can benefit various novel applications. Such applications can include microbiology, neuroscience [1, 2], non-contact optical manipulation at microscopic scales [3–5], cell sorting [6], materials processing [7], microfabrication [8, 9], controlled photo stimulation [1, 10], cell surgery [11], or advanced microscopy [12, 13], to name a few. Hence, alternative light shaping techniques that offer promising enhancements and are always being explored and developed.

Given such a variety in applications and methods, deciding which beam shaping technique works best for which particular application becomes an important task. For example, depending on the experiment, optical manipulation may either require strong gradient forces for position stability [14] or beams that can manipulate over extended regions [15]. Microfabrication, on the other hand, may operate with static beams but would require intense and highly localized light to trigger nonlinear process with high fidelity. In applications like photo-stimulation or neurophotonics, the tolerance of the beam profile to the perturbing biological media can be more important than either modulation speed or peak powers. Other applications that have an effective threshold to the light intensity, like optical trapping and some two photon processes may tolerate a noisy background. In addition to the application's requirements, practical constraints such as efficiency, budget or setup size are also important.

Hence, given the demands and diversity of applications that can benefit from laser beam modulation methods, the continued exploration of traditional light shaping modalities and the development of new ones can be as important as the applications where they are supposed to be used. Among the many requirements of laser applications, efficiency is one that can be easily understood and is always desirable. This is why "phase-only" techniques are preferable over amplitude modulation despite the simplicity of the latter. Phase-only techniques neither block light nor deflect it away in a subtractive manner in order to sculpt out the desired final pattern, but instead exploit interference and diffraction effects to modulate the available light.

Pre-defined phase distributions are usually applied using lenses, prisms, and phase-gratings which can now be found on many consumer devices. In research studies and high tech applications, it is a common objective to test many different and often novel phase distributions

Andrew Bañas: OptoRobotix ApS, DK-2000 Frederiksberg, Denmark
***Corresponding Author: Jesper Glückstad:** DTU Fotonik, Dept. Photonics Engineering, Techn. Univ. of Denmark, DK-2800 Kgs. Lyngby, Denmark, E-mail: jesper.gluckstad@fotonik.dtu.dk

"on-the-fly" without going through an otherwise expensive fabrication process. Hence, many laboratories utilize phase-only spatial light modulators (SLM) wherein a computer can control the individual phases of pixels on a reflective or transmissive surface. Besides the more familiar SLMs based on optically [16, 17] or electrically [18–20] addressed liquid crystals, alternative and promising devices for optical phase modulation such as deformable mirror membranes [21], MEMs-based piston-type mirror arrays [22] and photo-patterned liquid crystals [23], are also available or are in active development. These implementation choices further increase the number of potential practical applications where phase-only light modulation is beneficial.

2 Light shaping and light distribution

Despite the normally interchangeable terminologies we try to distinguish "light shaping" and "light distribution" in the scope of this review. This would help in telling apart the purpose of different techniques and also in appreciating their respective strongholds. So far, common light modulation techniques can be loosely classified based on whether they are utilized to distribute multiple beams in parallel or whether they shape the beams individually. For example, a collection of sparse focal spots in a 3D space, typically formed via diffractive optics or holography can be classified as a distribution. On the other hand, if we zoom into each of these focal spots in isolation, we can also characterize their individual form. We would refer to modifications on the form or structure of individual focal spots as light shaping. The spatial arrangement of a collection of "copies" of these focal spots or shaped point spread functions would be referred to as light distributions. As we shall see, both the collective spatial distribution of the beams and the shape of the individual beams have relevant roles.

In research applications such as optical manipulation [24] or biophotonics [1, 2], light has to be targeted to the dynamic distribution of the tissue or particles in the experiment. Other applications that emphasize the beam distribution include optical fractionation and parallel materials processing where a periodic array of beams is commonly utilized. In such applications, the actual shape of the beam being distributed is often ignored and it is enough that the typically Gaussian, Airy-disk or Sinc beam profile has the required size.

While a lot can be achieved with a simple focused beam, significantly more can be done by shaping these beams to something other than just a circular spot. There are situations where the illuminated objects are no longer "point-like" and greater control of the interaction between light and matter is required. Even if it is possible to scan a sharply focused spot over a shaped region of interest, this is not the same as having a spatially shaped single shot exposure. For example in STED microscopy [12], it is necessary to have a "donut" shaped light profile that suppresses fluorescence excitation except at the center of the donut. The amount of refraction, reflection or absorption in an optically manipulated particle will also vary throughout the particle's extent, depending on its structure [25] or composition which can also be engineered [26]. Moreover, in laser materials processing, it has been shown that tailored patterned beams can control the melt flow out and kerf [7]. Therefore, given more advanced applications, a typical center-weighted rounded beam profile would no longer necessarily be the most effective.

Another example of light shaping is the contiguous lateral shapes formed by GPC or even hard amplitude truncation. To further clarify the distinctions made in this review, we describe shaped light as typically having no gaps or discontinuities in their amplitude and phase like the examples mentioned. These distinctions are not exclusive to a given light shaping technique, and to certain extents different techniques can do both shaping and distribution. However, it is clear that some techniques can outperform the other in light shaping or light distribution.

2.1 Light shaping techniques

Amplitude modulation, wherein regions are removed from a broad beam, could perhaps be the simplest form of light shaping. It is fairly straightforward to implement and can be found on many common display devices. On the other hand, it is also well known to be the least efficient. Hence, in situations wherein there is limited laser power or in high power applications that also imply high power losses, phase-only alternatives are desirable.

Several efficient light shaping techniques can transform an available light source, typically a Gaussian beam, into a rectangle, circle or other simple shape while keeping a contiguous amplitude and phase profile. Other than GPC, examples include refractive mapping [27], phase plates [28, 29] or diffractive optical elements (DOE) [30, 31]. Refractive mapping redirects rays in a controlled manner such that the transformed output beam has a well-defined wavefront. DOEs or single phase plates use Fourier optics

principles to directly apply a Sinc or Airy disk-like phase distribution on an input Gaussian beam, which, in turn, becomes a top hat in the far field or after an additional lens [28].

Among existing phase-only options, GPC is a highly suitable replacement for amplitude modulation. In practice, GPC generated light distributions resemble that of simple amplitude modulation. Both are characterized by sharply outlined patterns with contiguous phase and intensity. However, these qualitatively similar techniques are opposites when it comes to photon efficiency. Whereas amplitude modulation blocks or absorbs light where darkness has to be defined, GPC utilizes destructive and constructive interference to respectively define darkness and re-channel photons in the foreground pattern.

2.2 Light distribution techniques

Given a single laser light source, one common task is to illuminate multiple separate locations. Hence, there are available light modulation techniques that re-distribute the light into multiple independently controllable beams. For example, beam splitters, gratings and diffractive optical elements, can be used to form a pre-defined static arrangement of smaller beams. High speed scanning mirrors can also make a single beam "appear" to be at different locations and can be good enough for certain applications such as displays and optical trapping at moderate speeds. Nonetheless, the advent of dynamically programmable phase-only spatial light modulators has opened many possibilities. Computer generated holography (CGH) or digital holography [32, 33] has traditionally been used with SLMs to address dynamic 3D distributions of focal spots. CGH output reconstructions are formed via optically Fourier transforming of light modulated by the SLM. The focusing nature makes digital holography ideal for creating 2D or 3D spot arrays useful for optical tweezing [3] or photo stimulation at different planes [10].

2.3 The "gray zone"

There are also cases wherein a distribution of countless smaller beams would take an overall shape. These are similar to individual pixels collectively forming a recognizable object in a computer screen. The fact that the pixels are tiny squares (or 3 RGB rectangles) becomes less important. Examples of beam shaping based on aggregating smaller beams can be found in static applications and include the use of engineered diffusers, micro-lens arrays or homogenizers [34, 35]. Engineered diffusers, micro-lens arrays and homogenizers work similarly by sampling an incident beam as a collection of beamlets that are then redirected to form an output shape. Due to the usual discontinuities of the adjacent redirected beams, these approaches are more suitable for incoherent light. The recombination of randomly phase shifted beamlets in spatially coherent light would create interference effects [36], resulting in speckled or grainy output intensities.

Despite the overlap in beam distribution and beam shaping, it is clear that there are approaches that outperform others in one of these aspects. Hence, this motivates the development of new light modulation techniques that can perform well in both light shaping and light distribution. Hybrid approaches are thus attractive for combining advantages from different techniques. As a primer to the hybrid techniques that will be covered later on, the proceeding sections will further discuss the operating principles behind digital holography and Generalized Phase Contrast.

3 Diffractive holography

Digital or computer generated holography is often used in optical trapping or optical tweezers and has been a typical application of phase-only SLMs as reconstructions can readily be visualized in the far-field or via a Fourier transforming lens. Computer-generated holography (CGH) extends Gabor's holography [37] to generate desired fields instead of simply reading out previously recorded information. But instead of using static holographic films for recording purposes, programmable spatial light modulators are used to dynamically emulate phase distributions that would synthesize the desired optical fields through interference and diffraction. Dynamically configured phase gratings synthesized using numerical or mathematical models eliminate the need for recording to holographic media. In most cases, the diffraction patterns formed at the output and the hologram drawn on the SLM are related via Fourier transform (Fig. 1), allowing fast and convenient calculations via the fast Fourier transform (FFT) [38].

The focusing geometry in digital holography effectively gathers a significant amount of light into individual spots, imparting a substantial power in the generated foci. In the simplest case, for example, all light falling on the SLM can be gathered into a single diffraction-limited spot. Using high NA objectives, such intense spots are useful for optical tweezing.

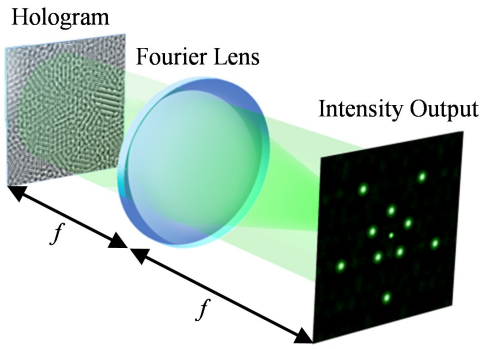

Figure 1: Holographic beam shaping based on a 2f geometry. Light whose phase is defined by the CGH is Fourier transformed to form target intensity patterns.

A common concern that needs to be dealt with when using holographic beam shaping is the occurrence of a strong zero order which is primarily due to limited fill factor and imperfections in SLMs [39]. Light falling into the non-addressable area, such as the dead space between pixels, would not be modulated, hence contributing to the zero order. The zero-order not only uses up light energy, it can also be disturbing to the sample if not dealt with. Besides simply utilizing a region away from the zero order, which would be inefficient, other ways of dealing with it includes blocking at a conjugate plane (e.g. [40]), adding a quadratic phase to the CGH to shift the output plane away from the focal plane [41], using a blazed grating to selectively deflect the higher orders, or destructive interference [39].

In order to fit the boundary conditions imposed by the fixed light source and the desired arbitrary output patterns, numerical calculations of non-trivial CGH distributions [42, 43] would be required. In the past, calculation speed of CGHs used to be a bottleneck for real time interactive output light re-configuration. However, the recent availability of parallel computing via graphical processing unit (GPU) [44] allows a single desktop/laptop computer to replace network linked parallel computers making it convenient for small laboratories. Instead of brute force optimization algorithms such as the Gerchberg-Saxton [42] or direct search algorithms [43], semi-analytic algorithms optimized for spot addressing can incorporate known effects of lens and prism phase distributions [45]. For example, holographic patterns can be actuated laterally by adding a linear phase ramp and axially by adding a quadratic lens-like phase to the CGH [45]. The addressing range of a holographic geometry would then be determined by the lens aberrations and the intensity envelope which depends on the SLM's pixel dimensions [46]. With more recent technology, digital holograms can be calculated as fast as around 2 milliseconds [47] with the experimental bottle neck being the SLM refresh rate.

Although some beams such as Airy, Bessel or Laguerre-Gaussian beams can be conveniently formed via digital holography [48], the creation of contiguous extended arbitrary areas of light would be a challenge in a $2f$ diffractive system given a fixed intensity input. A focusing geometry with a fixed illumination is inherently prevented from generating contiguous light patterns desirable for some applications. Extended intensity patterns formed by aggregating spots with differing phase values and overlapping point spread functions thus results in speckles that resemble noise [49]. The intensity fluctuations in speckled extended intensity patterns become a problem when they are enhanced by non-linear effects such as two-photon excitation such as in direct laser writing [50] or in two-photon optogenetics [2].

Contiguous patterns whose amplitude and phase are both well-defined would be imposing an input amplitude that usually does not match the typical laser source profile. In other words, the corresponding inverse Fourier transform of a given desired output is typically not well represented. Hence, when trying to recreate extended areas, output derived from numerical optimizations would tend to have spurious amplitude and phase discontinuities or speckle noise artifacts. Although it is possible to group multiple diffraction-limited holographic spots to collectively form a "shape", such aggregated spots are not likely to have the same phase and intensities. Such random looking phase of such light distribution also makes its propagation behavior less predictable. Such light patterns quickly degrade upon propagation due to interference from the randomized phase. This prevents use for applications like extended beam propagation.

Despite some of its limitations, diffractive approaches also have beneficial features that are not present in $4f$ mapping approaches such as GPC. The setup does not require a calibrated Fourier filter, hence slightly lowering the bill of materials, eliminating alignment requirements for the spatial filter and allowing more freedom in the scaling of the SLM patterns. More importantly, holography is capable of addressing multiple spots in a 3D volume, whereas GPC output is limited to a conjugate plane of the SLM.

4 Generalized Phase Contrast (GPC)

Generalized Phase Contrast [51] (GPC) is an extension to Zernike's phase contrast microscopy [52] primarily designed for beam shaping, but also finds use in quantitative phase imaging [53, 54], optical encryption [55] and even novel fields such as neuroscience [1] and even atomtronics [56]. GPC optically projects, typically user-defined, two-dimensional fields on an output plane. On the other hand, conventional phase contrast is typically used to visualize naturally occurring, thin and unknown phase variations. With its primary use on beam shaping instead of sample imaging, GPC emphasizes the efficient conversion of the phase input patterns into output intensity patterns. Subsequent to the initial proposal of using GPC in image projection [57] and its experimental demonstration for the efficient projection of binary images [58], GPC has been successfully developed and shown to be a viable dynamic projection technology, especially for real-time interactive micro-manipulation [4]. GPC can project grayscale lattices [59] and is suitable for efficient laser projection of grayscale non-periodic patterns and images [60, 61]. It can also accommodate non-uniform profiles, such as Gaussian beams [62–65].

GPC operates as an efficient non-absorbing common path interferometer [66]. A GPC setup is shown in Fig. 2 where a phase-only aperture directly representing the desired output intensity is imaged through the interference with a synthesized reference wave (SRW) resulting from the phase-shifted low spatial frequencies. The phase shifting of the lower spatial frequencies is achieved through a phase contrast filter (PCF) at the Fourier plane. GPC could thus be implemented with binary phase plates that are far simpler than those used by other Gaussian transformers as demonstrated in [67] and will be presented later in the experiments. Binary phase plates are also easier to mass-produce with standard photolithography or etching processes commonly used for silicon devices or microelectronics. When the phase mask and PCF are designed to give the same phase shift, both can even be fabricated from a single wafer. Unlike DOEs, GPC uses the target shape to directly interface with the incident Gaussian, instead of the target's Fourier transform. This makes GPC robust to input beam variations. The use of common path interferometry renders steep well-defined edges in the shaped output. Furthermore, the target output shapes could easily be replaced without increasing the fabrication complexity of the phase aperture or PCF. GPC's use of an imaging geometry also avoids dispersion effects which makes it advantageous for use with multiple wavelengths [68, 69] or temporal focusing [1, 2] which can effectively confine light along the axial direction.

Since GPC directly maps an input phase pattern into an intensity pattern through a $4f$ configuration computational requirements are significantly lower, requiring only the direct re-positioning of mapped phase patterns instead of iterative Fourier transform calculations. This enables real-time reconfigurability of output even on modest computing hardware. Patterns are thus easily updated in real time giving more control when manipulating complex 3D microstructures [5, 24] or allowing use in conjunction with other high speed techniques. GPC's use with high speed galvanometric scanning mirrors, for example, allows trapping of massive arrays (14 × 14 microbeads) [70].

Unlike speckled or discontinuous patterns, light distributions with contiguous intensity and phase remain localized while propagating, enabling extended optical manipulation [4, 5, 24, 71]. The flat phase profile of the output also makes GPC convenient for certain volume oriented applications such as counter propagating optical traps [5, 72] that can catapult particles to a height of ~100 μm. With its contiguous, speckle-free patterns and computationally simple SLM encoding, GPC therefore finds more uses in contemporary applications besides optical trapping and manipulation [5, 24, 70] such as and two-photon optogenetics [1]. Numerical simulations and experiments (presented later) show that GPC can transform incident Gaussian beams with up to 84% efficient and the intensity gain can be up to ~3x [63].

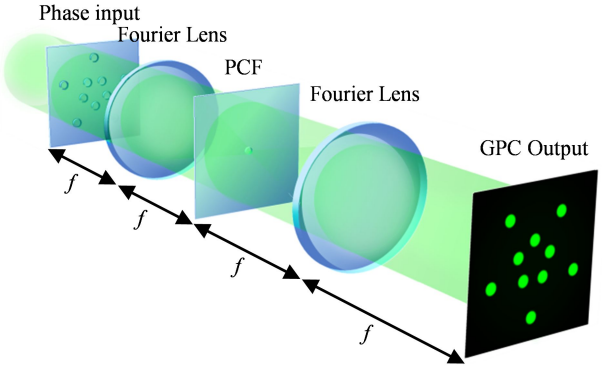

Figure 2: A Generalized Phase Contrast setup. Phase input patterns are mapped into output intensity patterns via common path interferometry. The PCF located at the Fourier plane shifts the input's lower frequencies that in turn serve as a reference wave, imaging the input phase pattern via interference.

4.1 Laser shaping applications that are not optimal for GPC

GPC is not without its shortcomings and there are applications wherein digital holography or other techniques, despite being more complex to implement, can be more practical when taking all things into account. Although GPC allows fast SLM addressing, its one-to-one pixel mapping sets an upper limit to how intense the output beam could be. GPC output can be up to 4 times more intense than the input level, corresponding to the constructive interference of the foreground pattern with the synthetic reference wave [51]. Holography's focusing geometry, on the other hand, allows larger regions of the SLM to be integrated into intense focal spots. Furthermore, although GPC can address multiple smaller beams, the working area is limited by the size of the imaged SLM plane. Even in a low NA counter-propagating optical trap setup, the smaller beam size and 3D addressing offered by holography can enable more efficient light coupling into 3D-maneuvered waveguide microtools [73]. These limitations in peak intensities and lack of 3D addressing have thus motivated the development of hybrid techniques such as matched filtering GPC [74] and Holo-GPC [75] that will be discussed later.

4.2 GPC theoretical background

When implementing a GPC system, the first practical step is to determine the best choice of phase mask and PCF dimensions given the wavelength, input beam diameter and other setup constraints. If the PCF is already fabricated for a given wavelength, the other options are to scale the input illumination (and illuminated phase mask) or the focal length to maintain a consistent scale at the filtering plane. Given these knowledge about the setup, we can summarize how to choose optimal phase masks and PCF sizes based on the formulations in [63] – all currently based on π-shifting phase values.

Given a Gaussian beam with a $1/e^2$ radius, w_0, illuminating a phase mask with phase profile $\phi(x, y)$, we define its normalized Fourier zero order, $\overline{\alpha}$, as

$$\overline{\alpha} = \frac{1}{\pi w_0^2} \int\int \exp\left[-(x^2+y^2)/w_0^2\right] \exp[i\phi(x,y)]dxdy. \tag{1}$$

In the absence of an input phase mask, the input Gaussian illumination would be transformed into a Gaussian focal spot at the Fourier plane. Assuming a wavelength, λ, and focal length, f, the Gaussian waist radius at the Fourier plane, w_f, is given by

$$w_f = \lambda f/(\pi w_0). \tag{2}$$

The phase contrast filter's π-shifting region's radius, Δr_f, is measured relative to this Fourier Gaussian, and is characterized by the dimensionless η given by

$$\eta = \Delta r_f / w_f \tag{3}$$

By imposing amplitude matching with a synthetic reference wave [76] for optimal interference, and that Δr_f coincides with the Fourier distribution's zero crossing [63] similar to holographic techniques, the conditions for optimal contrast and efficiency of the GPC output lead to the following equations

$$\eta = \sqrt{-\ln\left(1-\sqrt{1/2}\right)} = 1.1081, \tag{4}$$

$$\overline{\alpha} = \sqrt{1/2} = 0.7071. \tag{5}$$

Equations (4) and (5) summarize the conditions for an optimally performing GPC system under Gaussian illumination. The fixed value for η in Eqn. (4) means that a reconfigurable GPC system with a fixed PCF will consistently perform optimally with different phase masks satisfying Eqn. (5). The phase mask's geometry, $\phi(x, y)$, should thus be tweaked such that Eqn. (5) is satisfied. For simple shapes such as a circle and a rectangle, we have analytically shown how to scale $\phi(x, y)$ such that $\overline{\alpha} = \sqrt{1/2}$ in [63]. These conditions are used for fabricating static glass filters, and for programming a dynamic SLM in experiments.

4.3 GPC experimental demonstrations

To test the applicability of theoretically derived design formulations, we demonstrate both static and dynamic implementations of GPC [64]. A practical method for calibrating the PCF's axial position and its interesting capability for shaping destructive interference [77] will also be shown. The light shaping experiments give about ~80% efficiency, ~3x intensity gain, and ~90% energy savings which are in good agreement with the theoretical estimations.

Although our demonstrations are designed for specific wavelengths and input beam sizes, implementations that allow more input freedom, have also been demonstrated recently [78, 79] and were achieved with an adaptive PCF. Hybrid light shaping techniques where the filtering plane is on an SLM would also benefit from having a tunable PCF.

4.3.1 GPC component calibration using shaped destructive interference

Based on the theoretical formulations, the PCF would typically have a shifting region that would be several to tens of microns in diameter. If the focused light misses this shifting region, filtering would not take place, and a GPC setup would effectively be reduced to a simple $4f$ imaging setup. Furthermore, since the focused beam spot diverges away from the focal plane, it is necessary to have the PCF to be positioned as close as possible to the focal plane. These requirements may seem trivial at first, but these alignments can take some time when building a setup. Hence, it is beneficial to have a procedure to speed-up the initial calibration.

Experimental calibration and alignment are usually guided by some output metric. Normally, GPC is configured to have constructive interference at the foreground. However, measuring the optimal brightness requires setting a reference. Instead of using the normally desired brightness as a calibration metric, we thus relied in a configuration that can reliably produce darkness, i.e. destructive interference.

Darkness is achieved by changing the foreground's fill factor relative to the Gaussian illumination. For a π-phase shifting circle phase mask, we found that darkness is generated when the phase mask radius is ~1.02 times the Gaussian $1/e^2$ radius. Similar to standard GPC, the defined dark regions are not limited to circular phase masks. Given a desired phase mask pattern, it should be scaled such that α'' is about -0.29 instead of $\sqrt{1/2}$. The corresponding SRW destructively interferes with the shaped foreground pattern (the negative sign is due to maintaining the shaped foreground as the π-shifted region which now has a larger contribution to α'').

Shaped darkness, or amplitude reversal [77], is also observed with an amplitude truncating iris. Such amplitude circular aperture should have a radius of ~$0.83w_0$. Although a truncating iris has the advantage of being wavelength independent, it is much easier to work with a transparent phase-only darkness mask as the observable peripheral light guides during rough alignment. Furthermore, a phase mask can be fabricated on the same wafer with the other input phase masks and PCFs, making it economical. For dynamic experiments, this means that the SLM can be used directly for calibration without adding extra components. Fig. 3(a)-(b) show GPC simulations using a darkness phase mask. Successfully reproducing this experimentally, as shown in Fig. 3(c) indicates that the components have been properly aligned and calibrated. Hence, the succeeding GPC experiments presented here used this calibration technique to precisely adjust the PCF's position. This has also been done on a setup with a dynamic SLM where interesting shapes can be encoded (Fig. 4). This alternate modality called "Dark GPC" [77, 80], makes it simpler to create extended regions of destructive interference or nodal areas by only using binary-only phase masks instead of using more complex iteratively optimized multi-level phase elements [81].

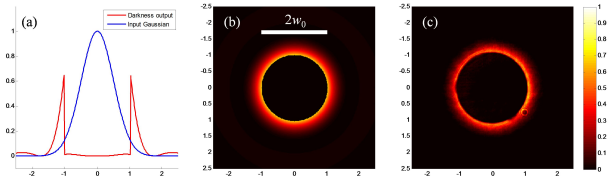

Figure 3: Relative intensity of a GPC generated darkness compared to the input Gaussian (a). Intensity profiles obtained from a simulation (b) and from experiment (c) (Figure adapted from [64]).

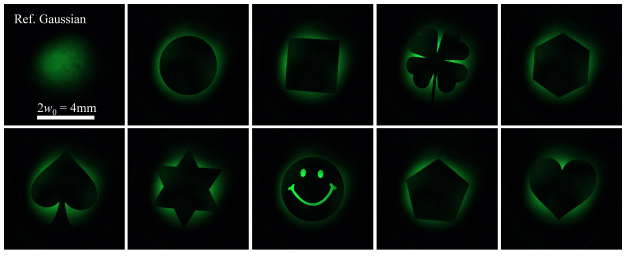

Figure 4: Shaped regions of destructive interference using different shapes encoded on an SLM (Figure adapted from [77]).

4.3.2 Static light shaping experiments

For our static light shaping experiments, we designed and constructed a GPC-LS to interface directly with a laser output having a 1mm diameter. Using two f = 50 mm Fourier lenses allowed us to keep the setup compact. The GPC-LS assembled with Thorlabs's half-inch optics and 16mm cage system is shown in Fig. 5. For more compact implementations, such as for OEM use, integrated micro-optics components [82] or alternative fabrication and assembly techniques can also be adopted.

We designed the phase mask and PCF for use with $2w_0$ = 1 mm, λ = 750 nm and f = 50 mm. The material used is fused silica (n = 1.454 at λ = 750 nm). The PCF's shifting

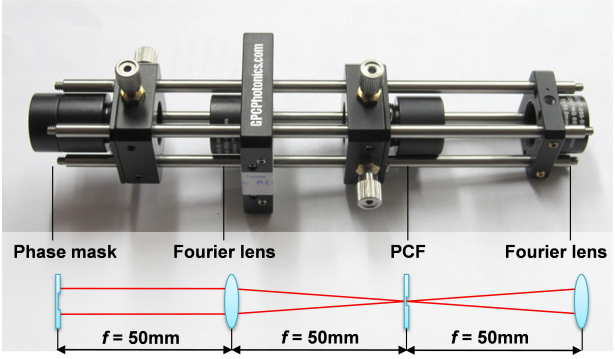

Figure 5: Pen sized GPC LS using two f=50 mm Fourier lenses and half inch optics assembly. (Figure adapted from [64]).

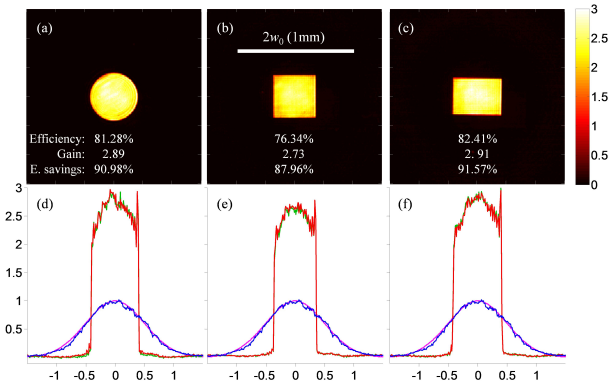

Figure 6: GPC intensity outputs from experiments for a circle (a), a square (b), and a 4:3 rectangle (c) phase mask. The scale bar in (b) is twice the $1/e^2$ Gaussian waist, and tick marks in (a)-(c) are separated by half the Gaussian waist. Efficiencies, gain and energy savings are also shown, and are consistently around ~80%, ~3x and ~90% respectively. The corresponding GPC intensity line scans are shown as green and red traces in (d)-(f) together with intensity line scans when simply imaging the Gaussian beam (blue). The axes are normalized relative to the Gaussian fit (magenta) and tick marks are spaced $w_0/2$ (0.25mm) apart (Figure adapted from [64]).

radius is calculated using Eqns. (2) to (4), hence,

$$\Delta r_f = \eta \frac{\lambda f}{\pi w_0} = \frac{1.1081 \times 0.75\mu m \times 50\ mm}{\pi \times 0.5\ mm} = 26.5\ \mu m. \quad (6)$$

The phase mask and PCF has an etch depth of ~826 nm to give a π phase shift. Conventional UV-lithography followed by wet etching in a buffered HF (BHF) was used to form the patterns.

For a circle or for rectangles, the phase mask size relative to the Gaussian beam diameter can be obtained from the tabulated ζ or ζ_{Rect} using the values derived from [63] and shown in Table 1. As an example, a rectangular phase mask with aspect ratio 4:3, the width has to be 0.4087 (ζ_{Rect}) times the beam diameter.

$$W = \zeta_{\mathrm{Rect}} \times (2w_0) = 0.4087 \times 1\ mm = 408.7\ \mu m \quad (7)$$

During assembly, we utilized the phase-only darkness calibration masks to fine tune the axial placement of the PCF. These masks were fabricated with a radius of 510 µm.

For our laser source, we used a supercontinuum laser from NKT Photonics that has a 1mm beam diameter. In our measurements, we used a 750 nm bandpass filter from Thorlabs with a bandwidth of 10 nm. This laser source is directed to the GPC LS. Output from the GPC LS is magnified (2x) then captured by a beam profiler (Gentec-EO). Different GPC output shapes were tested on the same GPC LS by interchanging the input phase masks. The efficiency, gain and energy savings results are summarized in Table 1.

Fig. 6(a)-(c) show GPC outputs for a circle, a square and a rectangle phase masks using optimized parameters listed in 4.3.3. The corresponding efficiencies, gain and energy savings are also shown for each shape and are consistently around ~80%, ~3x and ~90% respectively. The corresponding line scans are shown in Fig. 6(d)-(e). Two output measurements were taken (red and green plots) and measured against the reference Gaussian (blue plot). A Gaussian fit (magenta) is used to normalize the axes in Fig. 6. There is an observable intensity curvature in the GPC output, but this is flatter than what can be attained from a hard truncated Gaussian [62]. If a flatter intensity is critical, a phase mask with an intensity compensating phase curvature [83] may be used with the GPC LS.

4.3.3 Dynamic light shaping using a spatial light modulator

We now show how GPC is applied for dynamic light shaping. The setup used for generating arbitrary GPC output shapes is shown in Table 1.

We used a phase-only SLM (Hamamatsu Photonics) that has an area of 16×12 mm^2 and pixel pitch of 20 microns. The SLM was illuminated with a 532 nm diode laser module, horizontally polarized and expanded such that $2w_0$ = 4 mm (200 SLM pixels). The Fourier lens used has a focal length of 100 mm. Here, we used a PCF with Δr_f = 9.4 µm which is relatively small due to the larger area of the SLM. The etch depth was ~577 nm in fused silica (n = 1.46 at λ = 532 nm). The resulting dynamic patterns are captured with a CCD camera (JAI TM-1327GE).

Binary bitmap images, $b(x, y)$, were displayed on the SLM and mapped to 0 and π phase shifts. These images were pre-scaled to satisfy Eqn. (5). GPC results for various

Table 1: Experimentally measured efficiency, intensity gain and energy savings of GPC shaped light compared with a hard truncated or amplitude masked Gaussian for a circle and different rectangles.

Shape or aspect ratio	ζ or ζ_{Rect}	Width or Diameter (μm)	GPC eff (%)	GPC gain	Amp masking eff (%)	E. savings (%)
Circle	0.3979	397.9	81.28	2.89	28.15	90.98
Square	0.3533	353.3	76.34	2.73	27.97	87.96
4:3 Rectangle	0.4087	408.7	82.41	2.91	28.31	91.57

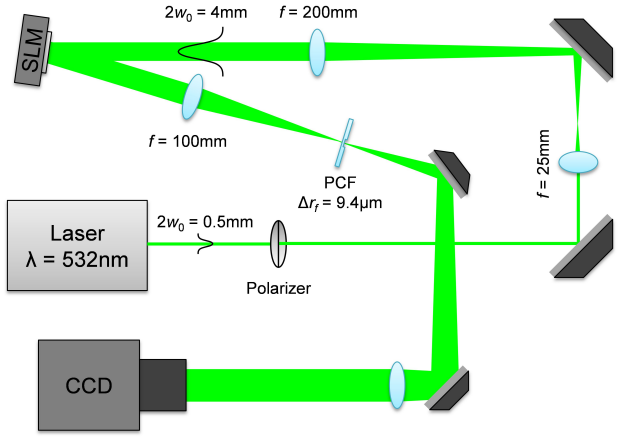

Figure 7: GPC LS setup with Gaussian illumination on a dynamic spatial light modulator (SLM). The SLM is illuminated with horizontally polarized Gaussian beam ($2w_0$ = 4 mm). The phase-modulated beam enters the GPC system (f = 100mm and f = 150mm Fourier lenses) whose output is imaged onto a CCD camera (Figure adapted from [64]).

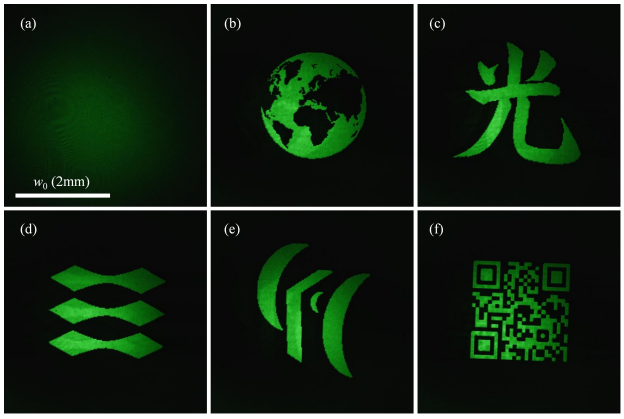

Figure 8: GPC generated arbitrary patterns obtained from experiments. The patterns are optimally scaled and then drawn on a phase-only SLM. A GPC LS after the SLM maps the phase patterns into intensity (Figure adapted from [64]).

optimized images are shown in Figure 8 together with the unmodulated Gaussian beam for comparison (Figure 8(a)).

Some applications require arbitrary light patterns and scaling these patterns is not an option. For example, in biological or optical manipulation experiments, the light has to match the samples that are present in the setup. In these cases, $\overline{\alpha}$ is kept at its optimal value by addressing an additional outer phase ring [63]. The intensity beyond this radius is considerably lower than that in the utilized region due to the roll-off of the Gaussian tails. Results for the ring-compensated neuron-shaped patterns are shown in Figure 9. Figure 9(d)-(f) show the possibility to optimally illuminate a brain cell that is branching out.

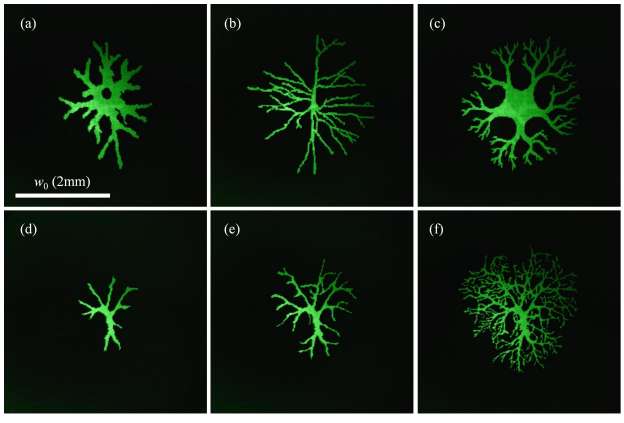

Figure 9: (a)-(c) Experimental results showing GPC generated intensity profiles of various neuron-inspired shapes, directly drawn on an SLM without scaling, but $\overline{\alpha}$-compensated by an outer phase ring. (d)-(f) Snapshots from a pattern that is branching out (Figure adapted from [64]).

4.3.4 Multi-wavelength light shaping

It has been previously shown theoretically and numerically that GPC shows robustness to shift in wavelength and can maintain both projection length scale and high efficiency over a range $[0.75\lambda_0;1.5\lambda_0]$ with λ_0 as the charac-

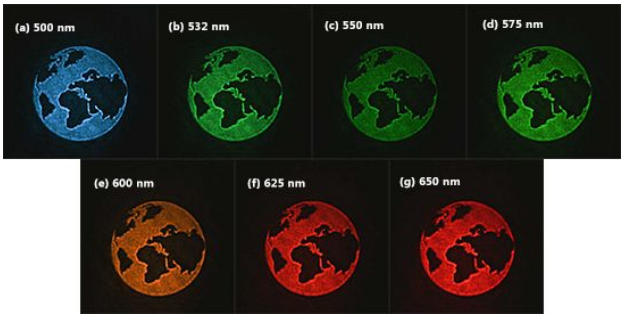

Figure 10: Color CCD images of GPC projections from the same setup, as the wavelength selector is varied from 500 nm-650 nm.The power at different wavelengths are adjusted individually for visibility. The input Gaussian beam size exhibits some wavelength dependence (Figure based on results from [69]).

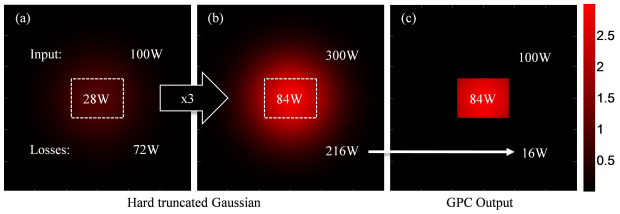

Figure 11: Comparison of GPC light shaping to a hard truncated Gaussian delivering 84W on identical rectangular areas. Being only 28% efficient (a), the truncated Gaussian requires 300W and loses 216W (b). The GPC light shaper requires only 100W, saving 200W (c) (Figure adapted from [63]).

teristic design wavelength [68]. As it turns out, the combined effects of identically phase-shifting phase mask and PCF pairs maximizes the destructive intereference of the SRW with the corresponding output background light [63, 68, 69]. This holds even if the phase shift deviates from pi upto a certain extent, as in the case of using a wavelength that is different to what the phase mask and PCF are fabricated for. With the resulting performance across multiple wavelengths and the recent availability of tabletop supercontinuum lasers, GPC light shaping opens the possibility for creatively incorporating various multi-wavelength approaches into spatially shaped excitations that can enable new broad-band light applications. Using a supercontinuum laser, we therefore present experiments showing GPC light shaping over a broad wavelength range [69].

To demonstrate multi-wavelength light shaping, we used a similar static GPC-LS setup, designed for a 1 mm input beam diameter, but centered at λ_0 = 532 nm. Light of different wavelengths is provided by a supercontinuum laser (NKT Photonics SuperK) then selected using a wavelength selector (NKT Photonics SuperK Select) to select the desired wavelength. Output from the wavelength selector was collimated with ~1 mm beam diameter using a fiber delivery system (NKT Photonics SuperK Connect).

The efficiencies and energy savings and observable output contrast across different wavelengths were within acceptable experimental variations, indicating the tolerance of the GPC LS. Figure 10 presents a globe pattern obtained at different wavelengths. The laser's power was adjusted for different wavelengths to maintain fairly uniform image brightness for the color CCD captures.

These results experimentally verify GPC's robustness to wavelength changes predicted by simulation data from previous theoretical analysis [68]. Analysis of measurements taken at different wavelengths show that the intensity gain was maintained at the level of ~3x throughout the wavelength range.

4.4 Using GPC to efficiently read-out holograms

As stated earlier, GPC's photon efficiency is typically over ~80%. On the other hand, amplitude modulation typically has a low efficiency, directly proportional to the encoded pattern's fill factor. Hence laser applications that normally use a hard-truncated amplitude shaped distribution of light are good candidates where the GPC-LS would be a beneficial alternative. Such is the case when using rectangular modulators with round Gaussian laser sources [84].

To quantify GPC's benefits over amplitude modulation, we consider GPC's efficiency and relative intensity gain. These two interdependent variables can be conveniently combined by defining the energy savings. This is the energy saved when replacing an amplitude masking system with a GPC system that gives the same brightness. This definition is illustrated in Figure 11 where both light shaping techniques are used to deliver 84 watts within a rectangular region. While an 84% GPC system would require 100W and lose 16W, a 28% efficient hard truncated Gaussian would require 300W and lose 216W. Hence, using a GPC system saves 200W or 93% of photon energy losses in a typical amplitude masking approach. Examples of experimentally obtained energy savings for different illumination geometries are shown in Table 1 together with the results from the static light shaping experiments.

To demonstrate the optimal illumination of an SLM, the output from a GPC light shaper with a 4:3 rectangular phase mask is used to illuminate a phase-only SLM with a 9.9 mm × 7.5mm active area (Hamamatsu Photonics) as shown in Figure 12. The benefits from matched illumination are then demonstrated by encoding computer gener-

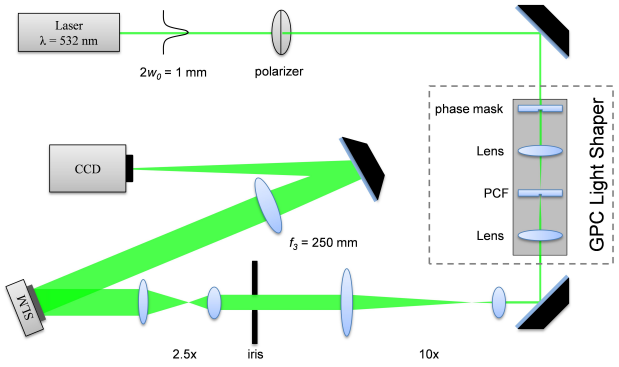

Figure 12: Setup showing how inserting a GPC-LS in the path of the light source can increase the output intensity or brightness in a CGH setup (Figure adapted from [84]).

ated holograms on the SLM for reconstruction with a standard 2*f* Fourier transform configuration.

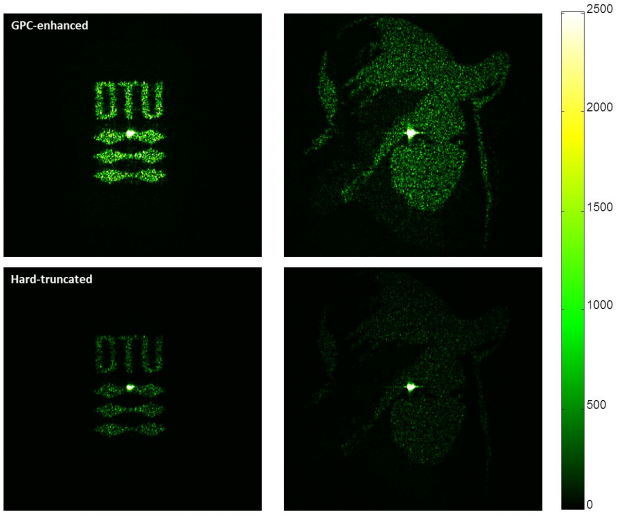

Figure 13: Holographic reconstructions with SLM illumination based on a GPC light shaper (top row) and a hard truncated Gaussian (bottom row). Both cases exhibit identical speckle distributions but there is a noticeable gain in intensity for the GPC-enhanced case. Color mappings are adjusted to improve overall contrast (Figure adapted from [84]).

The GPC light shaper used is similar to that used in static experiments shown earlier with a phase mask and PCF designed for 532nm illumination wavelength. The GPC generated 4:3 rectangle was then expanded to match the SLM area. For reference, the GPC-LS is disabled by displacing the phase contrast filter (PCF) to generate a Gaussian that is then hard-truncated. The input laser power level is maintained for both GPC-amplified and hard truncated illumination.

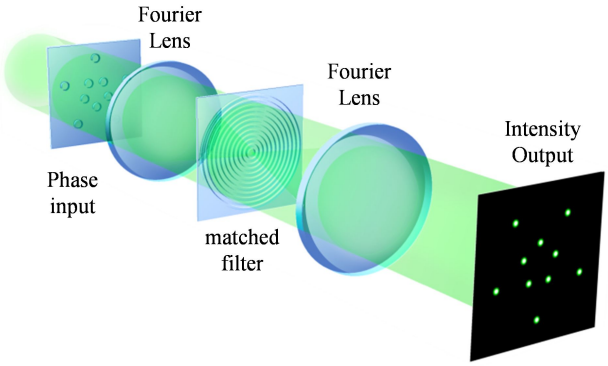

Figure 14: Setup for mGPC. Input circular phase patterns are mapped into intense output spikes by combining the operating principles of GPC and phase only correlation. The matched filter contains concentric rings that coincide with the Airy-like function's lobes.

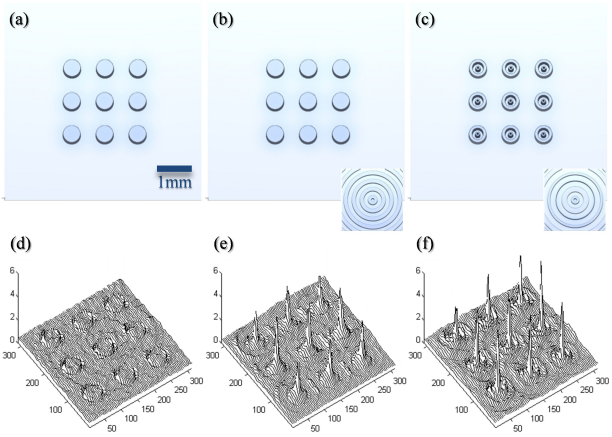

Figure 15: Example mGPC input phase patterns consisting of 53 pixel diameter disks and the resulting output without Fourier filtering (a & d). Output with applied matched Fourier phase filtering (c & e). Output using a GS-optimized correlation target pattern with the same input diameter pattern (d & f). Insets in (b) and (c) show the binary-phase matched filters used. (Figure based on [91]).

The GPC illuminated hologram on the top row in Figure 13 shows noticeably much brighter reconstructions with better contrast compared to the bottom row where conventional illumination is used. It is important to note that the aside from brightness and overall efficiency the reconstructed intensities are practically identical for both illumination cases. These results show that the same experiments could be done with a 1/3 less powerful laser. Alternatively, a 3x larger working area or 3x more focal spots can be addressed for the same laser power when using a GPC-LS [85]. Hence, for SLM based experiments where light efficiency is emphasized, a GPC Light Shaper is a practical tool to get as much photons into the SLM to begin with, re-

gardless of what light shaping technique is subsequently done with the SLM.

5 Hybrid light shaping techniques

In the previous section we showed how using GPC can be beneficial in a holography experiment. The illumination of SLMs, however, is just a simple practical application of directly using GPC's shaped output. More advanced techniques can result from a synergistic combination of two or more efficient light shaping methods wherein their respective unique features are exploited to generate something that neither technique could have achieved alone.

As such, several light shaping approaches wherein the phase distribution is actively modulated in two or more planes have been proposed. These techniques operate by using output from one light shaping process as the input to another light shaping process. Perhaps the most familiar and most general is Bartelt's tandem configuration [86–88] which can be understood as a series combination of two holograms. One hologram reconstruction is utilized to read-out a second hologram. The read-out light for the second hologram can have arbitrary amplitude distributions, giving full control of amplitude and phase. The tandem approach proposes the active control of the phase distribution. Hence, the freedom in output distributions comes at the cost of using multiple active SLM surfaces which can increase diffraction losses and make alignment more challenging. It is interesting to note that dynamically shaped GPC output has also been proposed for hologram read-out for a configuration similar to Bartelt's [89]. Such configuration would be more robust as the flat phase of GPC's output eases alignment constraints between the readout beam and the CGH.

GPC and techniques deriving from it also define phase distributions at different planes. However, the filtering plane has always been a simple and fixed phase distribution that is practically implemented with a fabricated high fidelity filter that is re-used for different output configurations. The fabricated filter also significantly costs less compared to an SLM and normally doesn't have similar pixilation or polarization constraints.

5.1 Matched filtering GPC

If we consider the beam from GPC's filter plane, through the imaging (second) lens, then to the output intensity, it can be seen that this can also be treated as a Fourier transforming setup. But unlike a typical hologram setup that uses Gaussian or tophat illumination, we instead have the optical Fourier transform of the input phase mask. This illumination typically resembles a Sinc function, or an Airy disk. Furthermore, GPC's PCF phase shift is correcting the central part, such that it matches the phase distribution of an ideal Sinc function or Airy disk [63]. This phase shifting is very similar to how phase constraints are applied on a hologram to get a desired Fourier transformed output.

With this framework, techniques from holography can be applied to the later "half" of the GPC setup. One way to modify GPC while maintaining a very similar hardware footprint is to incorporate matched filtering. Like GPC, the Fourier spatial filter can be a fabricated static binary phase mask (Figure 14). Assuming a circular input phase mask, instead of phase shifting only the central part of the Fourier transform a filter can be designed to rectify the alternating signs of the Airy-disk-like lobes with matching concentric phase rings. This effectively emulates having a flat phase plane wave which makes the output resemble focal spots. Hence instead of tophats, mGPC output would be narrower beams with higher peak intensities.

Alterntively, mGPC can also be interpreted as applying a phase-only correlation on the GPC tophat output. Hence, by borrowing features from phase-only correlation, matched filtering Generalized Phase Contrast (mGPC) combines the respective strongholds and advantages of GPC and diffractive beam shaping (e.g. holography). Similar to GPC, mGPC does not suffer from a strong un-diffracted zero-order light, ghost orders and spurious phase variations. Likewise, it is also straightforward to encode SLM phase patterns, only requiring translated copies of the same basis shape. Due to the similar $4f$ geometries, mGPC shares GPC's advantages [90]. However, with the additional correlation part, mGPC also gathers light into strongly focused spikes without squeezing the field of view or working area in the sample.

As in image detection, the correlation part also makes mGPC tolerant to input noise such as mild phase aberrations, hence, being able to work even with consumer grade pocket projectors based on liquid crystal on silicon [91]. GPC, on the other hand, would also have revealed the surface imperfections of a consumer grade modulator.

Other methods can also be borrowed from digital holography. Instead of being limited to circular tophat patterns at the input plane and an Airy disk at the Fourier plane, it is possible to use other patterns with a broader Fourier transform. This ensures that higher frequency components necessary to define sharp features contribute more in the formation of the output. Knowing how the amplitude distributions should ideally look like at both the in-

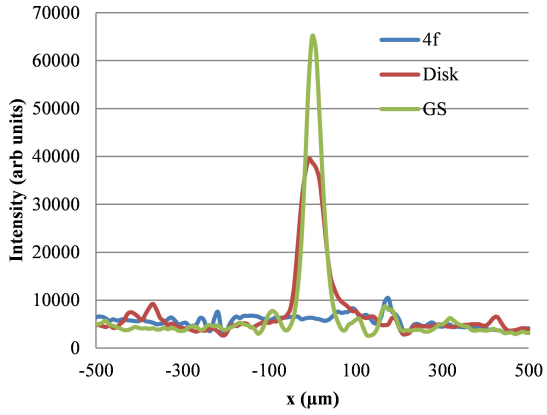

Figure 16: Line scans comparing the intensities of generated spot profiles. (Figure based on [91]). The disk based and GS optimized mGPC output have peak intensity gains 7.2 and 11.9 with respect to the average 4f imaging output.

put and Fourier planes, a phase retrieval algorithm such as the Gerchberg-Saxton (GS) algorithm [42, 43] can be used to optimize such input phase patterns.

5.2 mGPC experiments with pocket projectors

Since the integrating effect of holography can tolerate moderate imperfections in the LCoS's phase flatness, relatively low cost consumer projectors can be operated as binary phase modulators with the proper choice of illumination polarization [92] which is −45° in our setup. The projector we used has an LCoS manufactured by Syndiant (model SYL2043) and has 800×600 pixels with a pitch of 9.4 μm [93]. In our demonstrations, we have successfully used a second LCoS and a pre-fabricated phase filter at the Fourier plane. Having a dynamic device as the matched filter makes initial tuning and optimization easier.

Input phase disks with a 53 pixel diameter were encoded in the first LCoS. The directly mapped image and mGPC outputs are shown in Figure 15. For the same disk diameter an increase in the peak intensity and a narrower spike is observed when using a GS-optimized input phase pattern and corresponding matched phase filter as shown in the superposed line scans in Figure 16. The disk based and GS optimized mGPC output show peak intensity gains of 7.2 and 11.9 respectively when compared to the average 4*f* imaged output.

Although typical consumer projectors only have black and white states, intensity modulation can be achieved via pulse width modulation. This is normally used to define states between black and white which are visually perceived as shades of gray via time integration. Using an oscilloscope and photo detector, we have verified that the LCoS we used switches at 180 Hz, which is consistent on how it switches between red, green and blue imaging channels while having a typical 60Hz color image frame rate. Figure 17 shows output showing different average intensity levels by encoding grey patterns into the LCoS.

Since video frame switching rates are typically far above required refresh rates for stable optical trapping and manipulation (~5-20Hz) [94], it can be expected that this time integrated intensity modulation would not be an issue for applications that don't require very high position stabilities like mechanical cell handling or cell sorting [6, 95] or microscopic illumination applications. By programming a scanning motion such spot arrays can also be used for microscopy applications [13].

To subsequently take advantage of a fixed filter pattern, we used a fabricated Pyrex filter optimized for a 50 pixel (475 μm) diameter filter in the mGPC experiments. The patterns in the matched filter are scaled to match the corresponding Airy disk produced with $\lambda = 532$ nm, and an $f = 300$ mm Fourier lens. This Fourier plane Airy disk has a central lobe diameter of 821 μm and concentric rings located at ~337 μm radius intervals. The GPC central phase dot (PCF part) has a radius of 21.46 μm chosen to give optimal contrast when the 5.7 ×5.7 mm^2 area (600 ×600 px^2) of the LCoS is illuminated with a tophat beam. The filter is then clamped near the back focal plane of the objective lens ($f_2 = 8.55$ mm, NA = 0.4) which in turn performs an inverse Fourier transform of the filter plane.

As spot patterns have already been presented earlier, we show the generation of "line patterns" that are useful in certain applications, e.g. for photo-excitation of extended segments of neurons [1, 10], faster 2PP microfabrication or structured illumination microscopy. Instead of distinct circles, line patterns with a thickness matching the prescribed diameter of the input disks are encoded at the SLM input phase (Figure 18).

Since a line can be considered as a collection of closely packed disks, the intensity becomes weaker as each disk takes away energy from its neighboring disks. Figure 18 shows sample phase inputs containing line patterns of letters forming "DTU" and "PPO", and the resulting intensity patterns that are generated when these phase patterns are used with mGPC. Points where the lines end or intersect need to be dealt with as the correlation with a disk respectively gives a stronger or weaker peak in these regions. For example, the line ends may be drawn less circular to suppress the correlation peak. If a multi-level phase SLM is

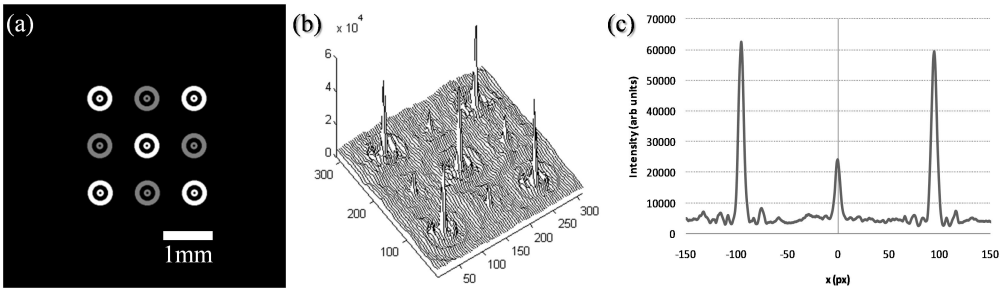

Figure 17: Correlation target patterns optimized via the Gerchberg-Saxton algorithm wherein some of the patterns have 50% gray levels encoded (a). The resulting optical output with intensity variations corresponding to the gray-levels encoded (b and c). (Figure adapted from [91]).

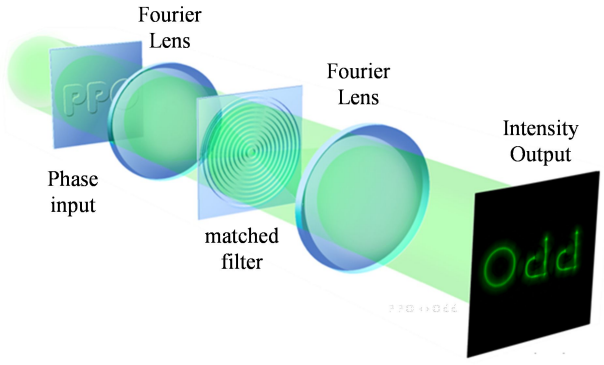

Figure 18: A 4f mGPC setup wherein extended line patterns are encoded in the input phase. Instead of discrete spots, sharp line intensity patterns are formed at the output.

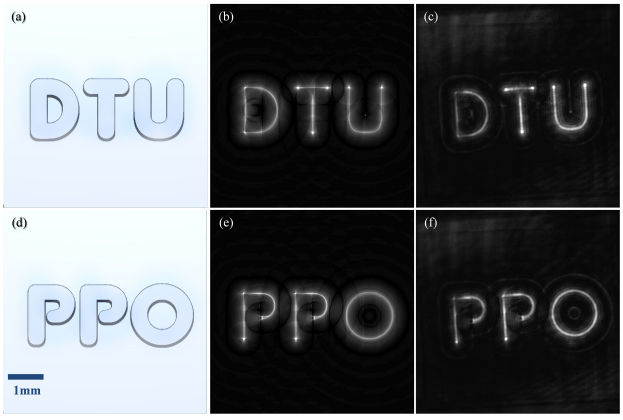

Figure 19: Generation of line patterns from letters forming "DTU" and "PPO". Binary phase patterns encoded at the pico projector LCoS SLM, (a) and (d), are shown with corresponding numerically calculated output intensities, (b) and (e), and experimentally reconstructed intensity patterns (c) and (f). (Figure adapted from [96]).

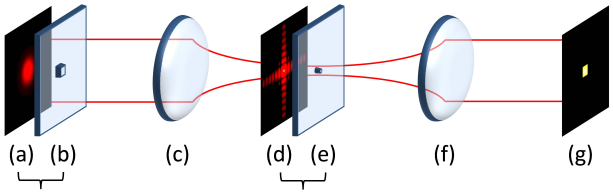

Figure 20: Standard GPC setup consisting of an input phase mask (b), Fourier lenses (c) & (f) and a PCF (e). The input illumination (a), its Fourier transform, after applying the phase mask (d) and the imaged intensity (g) are also shown (Figure adapted from [75]).

used, the variations in intensity may be compensated for by encoding different phase levels.

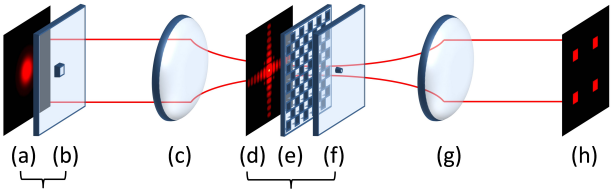

Figure 21: Holo-GPC setup. Compared to standard GPC, a hologram (e) is placed in addition to the PCF at the Fourier plane of the first lens. For practical implementations, the hologram is typically encoded on an SLM, and the sizes of the input beam, phase mask, PCF and focal lengths have to be adjusted. The second lens (g) optically Fourier transforms the light that is altered by the hologram and PCF to get a distributed output consisting of speckle-free contiguous shapes (Figure adapted from [75]).

5.3 Comparing mGPC with normal focusing

Matched filtering GPC offers some advantages over digital holography. Similar to GPC that uses an imaging geometry, the output is easily reconfigured by positioning the corresponding input disks. This also means that there is

no need for more advanced techniques or computing resources to calculate holograms in real time. High speed binary-only SLM's can also be utilized without suffering from ghost orders or a strong undiffracted zero-order, as we have demonstrated. However, when it comes to focusing strength, mGPC will not outperform a hologram that is illuminated with a broader top-hat or Gaussian beam. The output of mGPC is also constrained in the imaging plane, unlike in holography where spots can be distributed over a 3D volume.

6 Holo-GPC

We have so far briefly discussed several hybrid light shaping approaches and showed how GPC can be used beyond reading-out a hologram with its direct output as in mGPC. While being relatively simple to implement, mGPC doesn't fully exploit the benefits of digital holography. Both GPC and mGPC, only a have a fixed element on the Fourier plane which is the PCF or matched filter. This fixed Fourier filter makes both of them practical to implement with only a single SLM required for dynamically reconfigurable output. The fixed matched filter in mGPC also makes its holographic features very limited. As Bartelt [89] suggests however, there are far more possibilities if the phase element at the Fourier plane can also be dynamically controlled. Indeed, near ideal arbitrary complex fields [88] can be generated when using a tandem of two dynamic SLM surfaces.

Holo-GPC offers an approach that technically can be considered a special case of a Bartelt tandem configuration (as with other 4*f* filtering based techniques). However, we prefer to maintain the practicality of requiring just one active SLM. Unlike other proposed tandem configurations, the first hologram is replaced by a well-defined, easily fabricated, and generally reusable phase mask. In the usual tandem configuration, the first phase element being a hologram generally bears no resemblance to the final output and would require re-calculation for different outputs. Pre-fabricated phase elements would be impractical as they cannot be specified with a few parameters, require multiple phase levels to be efficient and would have to be replaced for each new output configuration.

6.1 Efficient and practical modification of the read-out beam

Just as the shape of generated individual output beams can be important, so is the shape of the light that is illuminating a hologram. Ultimately, the read-out illumination determines the amplitude and phase distribution of the point-spread function (PSF) at the output optical far-field plane. We are particularly interested in modifying the "spread function" of the output beams. As the typical illumination shape would have a tophat or a Gaussian distribution, the typical PSFs are either shaped as Airy-disks or Gaussians. The target output PSF can thus be changed by illuminating with an (inverse) far-field transformed beam shape. The challenge, therefore, is the efficient creation of an initial basis beam shape (typically using the Fourier transform) that will become the output's PSF. This goes beyond mGPC where only the phase of the ideal plane wave is simulated.

It is well known that a Fourier transformed amplitude mask can be used to illuminate a hologram in order to get PSFs with the same amplitude pattern. Holo-GPC starts with a similarly looking phase mask that efficiently transmits the input light without absorbing photons. But unlike a straight-forward convolution, phase filtering is required to convert the phase mask into shaped PSFs at the output. As it relies on GPC's phase to intensity mapping, Holo-GPC also inherits GPC's efficiency advantage over amplitude masking and would in principle also have 3x brighter PSFs or over 90% of energy savings [63].

6.2 How Holo-GPC works

To understand how Holo-GPC works, we first briefly revisit the standard GPC configuration and subsequently identify the modifications necessary to make multiple holographic copies of this GPC output. In a standard GPC setup (Figure 20), the input phase mask is first optically Fourier transformed and the resulting distribution is focused on a phase contrast filter (PCF). An output intensity mapping of the input phase mask is generated from the interference of the imaged input with a so-called synthesized reference wave (SRW) that results from the low frequency components phase shifted by the PCF.

Just as with mGPC, we treat the region between the PCF plane, through the imaging lens, then to the output intensity (Figure 20(d) to (g)), as a Fourier transforming configuration. The optical Fourier transform of the input phase mask can be thought of as the illumination at this plane. For a rectangular or circular input phase mask, this PCF illumination typically resembles a Sinc function, or an Airy disk, but in general, this can be the Fourier transform of the desired PSF-shape with similar geometry as the input phase mask. As with holography, the PCF's phase shift is correcting the central part, such that it matches the

phase distribution of an ideal Sinc function, Airy disk [63] or Fourier transform of the desired PSF pattern. Hence, through convolution, by placing a hologram phase on top of this PCF-shifted, Fourier-transformed phase mask, Holo-GPC can produce a beam distribution wherein each beam takes the form of the intensity mapped input illuminated phase mask as in Figure 21.

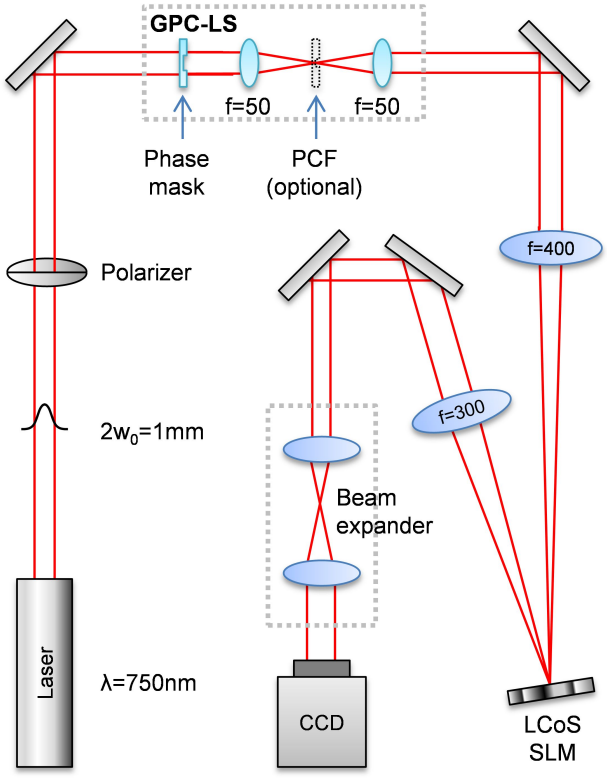

Figure 22: Optical setup for Holo-GPC experiments (Figure adapted from [75]).

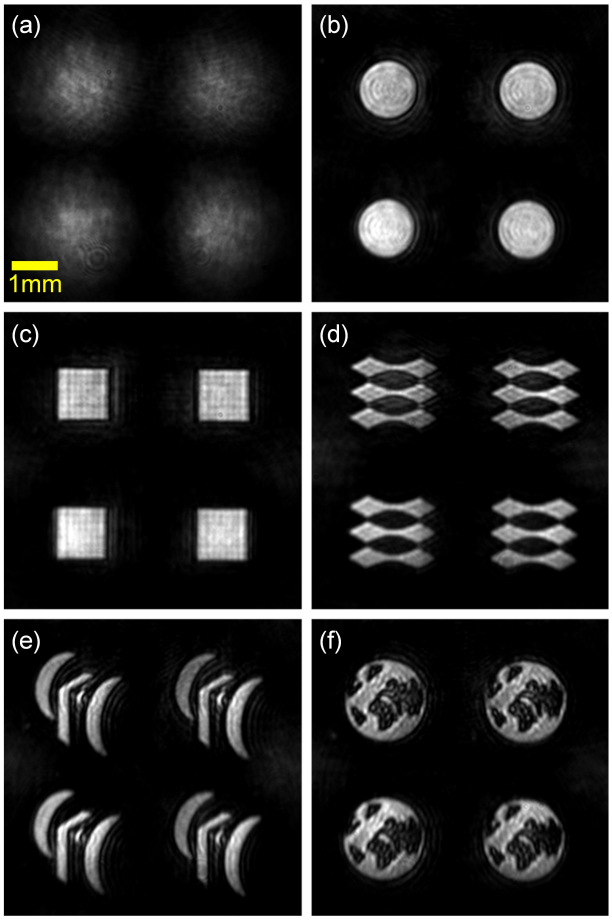

Figure 23: Initial holographic output from a checkerboard grating (a), then with Holo-GPC encoded with different phase masks (b)-(f). The scale bar corresponds to 1 mm at the camera (Figure adapted from [75]).

As Holo-GPC operates by efficiently modifying the point spread function, the individual beams are identical copies of the intensity-imaged phase mask pattern. This multi-beam approach is a different paradigm from standard GPC wherein a phase mask utilizes multiple smaller sub-shapes that need not be identical, and hence the corresponding output individual beams can also have different shapes. However, unlike standard GPC, Holo-GPC's output beams are not constrained to an imaging plane, but rather, can be addressed in a 3D holographic manner. Furthermore, a compensating phase mask region [1, 63] is not necessary for maintaining the optimal fill factor while changing the number of output beams.

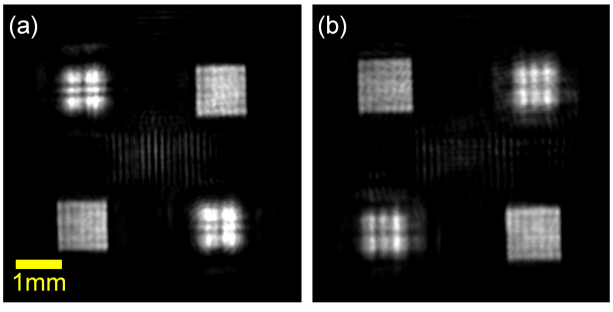

Figure 24: Holo-GPC addressing beams in 3D. Planes in (a) and (b) are 215 mm apart axially and include both "in focus" and diffracted "out-of-focus" square beam reconstructions (Figure adapted from [75]).

6.3 Holo-GPC experiments

Our preliminary setup is illustrated in Figure 22. We used a λ = 750 nm laser source (filtered supercontinuum laser from NKT Photonics) and re-purposed a static GPC-LS from the earlier experiments [64]. The PCF within the static GPC-LS is displaced from the beam path. An 8x magnified image of the GPC-LS's focal plane is used to illuminate a phase-only SLM (Hamamatsu Photonics, pixel pitch = 20 µm). The SLM-encoded PCF shifting region has a diameter of 21 pixels or 420 µm which is very close to the theoretical optimal 423.26 µm [63]. The complex field at the SLM plane is optically Fourier transformed with an f = 300 mm lens, then magnified for sufficient coverage of the CCD camera.

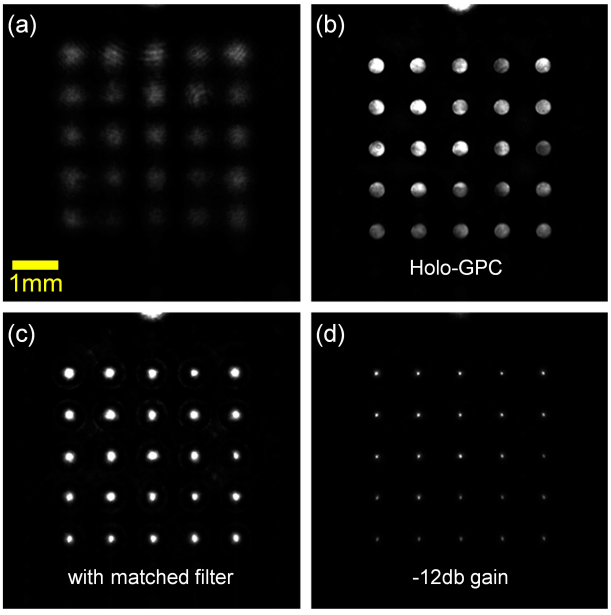

Figure 25: A 5×5 holographically diffracted Gaussian spot array (a) shaped into circles via Holo-GPC (b), then converted into intense spikes (c) via matched filtering. To reduce the saturation (d), the camera gain had to be 12db lower (Figure adapted from [75]).

For the holograms, we tested a simple binary checkerboard grating, multiplexed spots distributed in 3D and a spot array generator. The multiplexed spots are based on the lenses and prisms phases encoded on non-overlapping random SLM regions that are assigned to each spot. For visualization, a blazed grating was used to shift the spot patterns away from the zero-order diffraction. Uniform illumination was used in the CGH calculations. For a given CGH, different phase masks were used to form different PSF shapes.

The output reconstructions from the binary checkerboard grating using different input phase masks are shown in Figure 23. Some loss in sharpness and fringing can be attributed to the finite SLM window and lens apertures, but the input patterns remain recognizable. The same SLM hologram is used even for the arbitrarily shaped phase masks. Figure 24 demonstrates 3D addressing with Holo-GPC by using a multi-spot hologram and then imaging the reconstructed output at planes by translating the camera by 215mm. Despite some noise from the hologram among the individual beams, it is clear that the square mask is focused at different planes and exhibits expected diffraction patterns at the off-focus planes.

6.4 Bringing Back Focusing Using Matched Filtering in Holo-GPC

When operating a Holo-GPC setup, the focal spots have to be broadened in order to draw well defined shapes on top of them. As some applications require stronger focusing it would be convenient to be able to switch between shaped and focused spots without changing the lens magnification. One way to achieve this is to re-introduce matched filtering [97]. The concentric alternating phase rings of the matched filter are easily applied on top of the PCF and hologram encoded on the SLM. We demonstrate matched filtering using spot array holograms, iteratively optimized [42] from an initial Dammann grating [98]. Figure 25 shows an initial Gaussian beam array, transformed into circular top hats, then transformed into more focused spots using the matched filtering technique. Since the image gets saturated, the result is also presented at a lower camera gain. The easy switching from shaped beams makes matched filtering a convenient feature in a Holo-GPC setup and may give an extra "jolt" in optical manipulation applications [15], or higher intensities for secondary or non-linear effects in multi-functional setups [26].

7 Conclusions

We have presented a brief review of efficient phase-only light shaping techniques such as holography and Generalized Phase Contrast. Both techniques have been extensively applied in research such as optical trapping and manipulation, biophotonics and neuroscience. Undoubtedly, computer-generated holography and Generalized Phase Contrast are highly versatile techniques that are encountered in a plurality of applications. As these two light shap-

ing methods have beneficial features not present in the other, hybrids of these approaches can offer a plurality of interesting and novel applications or improve laser light utilization in current applications. In particular, we have cited how holography is more effective for distributing focal spots over a 3D working volume while GPC has its strengths in creating speckle-free, contiguous and well defined shaped beams.

Reflecting on the respective strengths of holography and GPC, we have thus developed a novel efficient phase-only light shaping approach that simultaneously controls the distribution of multiple beams and shape these beams individually. This new technique called Holo-GPC thus extends the capabilities of both GPC and holography. Holo-GPC is a hybrid of holography that can create extended 2D or 3D beam distributions and GPC that forms noise-free sculpting of the individual beams. Our preliminary experiments show how Holo-GPC is easily implemented with a phase-only SLM and simple binary phase patterns that determine the shape of the beams or PSFs. Instead of being limited to round spots with intensity roll-offs, Holo-GPC makes it possible to have spatially distributed structured beams with well-defined high contrast boundaries. The resulting shaped intensity profiles can provide more precision and contrast in applications such as laser materials processing or for two-photon optogenetics. If necessary, further improvements are possible by using an actual high fidelity PCF, and using more sophisticated hologram calculation algorithms. If the cost and efficiency trade-offs using an extra SLM are acceptable, having a dynamic input phase mask also significantly increases Holo-GPC's versatility. Special purpose lower resolution SLM's [99] can also be utilized for a small set of pre-defined shapes. We have also shown that one can easily switch between laterally shaped beams into more focused spots using matched filtering. This alternate matched filtering modality, further extends the versatility of a Holo-GPC system and makes it easier to adopt in existing holographic setups that require stronger focusing.

Acknowledgement: Work covered in this review have been supported by GAP funding from the Copenhagen Cleantech Cluster (CCC), the Enhanced Spatial Light Control in Advanced Optical Fibres (e-space) project Innovation Fund Denmark (Grant number: 0603-00514B) and the Combined Molecular Microscopy for Therapy and Personalized Medication in Rare Anaemias Treatments (CoMMiT-Ment) FP7 collaborative project (Grant agreement number: 602121). We thank our industrial collaborators; Hamamatsu Photonics K.K. Central Research Laboratory and NKT Photonics A/S. Our colleagues, Darwin Palima, Mark Villangca and Oleksii Kopylov contributed to different parts of the original work covered in this review.

References

[1] E. Papagiakoumou, F. Anselmi, A. Bčgue, V. de Sars, J. Glückstad, E.Y. Isacoff, V. Emiliani, Scanless two-photon excitation of channelrhodopsin-2, Nat. Methods. 7 (2010) 848–854. doi:10.1038/nmeth.1505.

[2] E. Papagiakoumou, Optical developments for optogenetics., Biol. Cell. 105 (2013) 443–64. doi:10.1111/boc.201200087.

[3] D.G. Grier, A revolution in optical manipulation, Nature. 424 (2003) 810–6. doi:10.1038/nature01935.

[4] P.J. Rodrigo, V.R. Daria, J. Glückstad, Real-time three-dimensional optical micromanipulation of multiple particles and living cells., Opt. Lett. 29 (2004) 2270–2. http://www.ncbi.nlm.nih.gov/pubmed/15524377.

[5] P.J. Rodrigo, L. Gammelgaard, P. Břggild, I. Perch-Nielsen, J. Glückstad, Actuation of microfabricated tools using multiple GPC-based counterpropagating-beam traps., Opt. Express. 13 (2005) 6899–904. http://www.ncbi.nlm.nih.gov/pubmed/19498709.

[6] A. Bańas, T. Aabo, D. Palima, J. Glückstad, Using pico-LCoS SLMs for high speed cell sorting, in: K. Dholakia, G.C. Spalding (Eds.), Proc. SPIE, 2012: p. 845838. doi:10.1117/12.930824.

[7] F.O. Olsen, K.S. Hansen, J.S. Nielsen, Multibeam fiber laser cutting, J. Laser Appl. 21 (2009) 133–138.

[8] S. Kawata, H.B. Sun, T. Tanaka, K. Takada, Finer features for functional microdevices, Nature. 412 (2001) 697–8. doi:10.1038/35089130.

[9] P. Galajda, P. Ormos, Complex micromachines produced and driven by light, Appl. Phys. Lett. 78 (2001) 249. doi:10.1063/1.1339258.

[10] M.A. Go, C. Stricker, S. Redman, H.-A. Bachor, V.R. Daria, Simultaneous multi-site two-photon photostimulation in three dimensions., J. Biophotonics. 5 (2012) 745–53. doi:10.1002/jbio.201100101.

[11] J. Ando, G. Bautista, N. Smith, K. Fujita, V.R. Daria, Optical trapping and surgery of living yeast cells using a single laser, Rev. Sci. Instrum. 79 (2008) 103705. doi:10.1063/1.2999542.

[12] S.W. Hell, J. Wichmann, Breaking the diffraction resolution limit by stimulated emission: stimulated-emission-depletion fluorescence microscopy, Opt. Lett. 19 (1994) 780–782. doi:10.1364/OL.19.000780.

[13] P.J. Smith, C.M. Taylor, A.J. Shaw, E.M. McCabe, Programmable array microscopy with a ferroelectric liquid-crystal spatial light modulator, Appl. Opt. 39 (2000) 2664–9. http://www.ncbi.nlm.nih.gov/pubmed/18345186.

[14] A. Ashkin, J.M. Dziedzic, Observation of Radiation-Pressure Trapping of Particles by Alternating Light Beams, Phys. Rev. Lett. 54 (1985) 1245–1248. doi:10.1103/PhysRevLett.54.1245.

[15] H.-U. Ulriksen, J. Thogersen, S. Keiding, I.R. Perch-Nielsen, J.S. Dam, D.Z. Palima, H. Stapelfeldt, J. Glückstad, Independent trapping, manipulation and characterization by an all-optical biophotonics workstation, J. Eur. Opt. Soc. Rapid Publ. 3 (2008) 8034. doi:10.2971/jeos.2008.08034.

[16] F. Li, N. Mukohzaka, N. Yoshida, Y. Igasaki, H. Toyoda, T. Inoue, Y. Kobayashi, T. Hara, Phase Modulation Characteristics Analysis of Optically-Addressed Parallel-Aligned Nematic Liquid Crystal Phase-Only Spatial Light Modulator Combined with a Liquid Crystal Display, Opt. Rev. 5 (1998) 174–178. doi:10.1007/s10043-998-0174-x.

[17] N. Mukohzaka, N. Yoshida, H. Toyoda, Y. Kobayashi, T. Hara, Diffraction efficiency analysis of a parallel-aligned nematic-liquid-crystal spatial light modulator., Appl. Opt. 33 (1994) 2804–11. http://www.ncbi.nlm.nih.gov/pubmed/20885639.

[18] Z. Zhang, Z. You, D. Chu, Fundamentals of phase-only liquid crystal on silicon (LCOS) devices, Light Sci Appl. 3 (2014) e213. http://dx.doi.org/10.1038/lsa.2014.94.

[19] N. Collings, T. Davey, J. Christmas, D. Chu, B. Crossland, The Applications and Technology of Phase-Only Liquid Crystal on Silicon Devices, J. Disp. Technol. 7 (2011) 112–119. doi:10.1109/JDT.2010.2049337.

[20] Y. Igasaki, F. Li, N. Yoshida, H. Toyoda, T. Inoue, N. Mukohzaka, Y. Kobayashi, T. Hara, High Efficiency Electrically-Addressable Phase-Only Spatial Light Modulator, Opt. Rev. 6 (1999) 339–344. doi:10.1007/s10043-999-0339-2.

[21] L.J. Hornbeck, Deformable-Mirror Spatial Light Modulators, Proc. SPIE. 1150 (1990) 86–103. doi:10.1117/12.962188.

[22] M. Hacker, G. Stobrawa, R. Sauerbrey, T. Buckup, M. Motzkus, M. Wildenhain, A. Gehner, Micromirror SLM for femtosecond pulse shaping in the ultraviolet, Appl. Phys. B. 76 (2003) 711–714. doi:10.1007/s00340-003-1180-0.

[23] P. Chen, Y.-Q. Lu, W. Hu, Beam shaping via photopatterned liquid crystals, Liq. Cryst. 43 (2016) 2051–2061. doi:10.1080/02678292.2016.1191685.

[24] D. Palima, A.R. Bańas, G. Vizsnyiczai, L. Kelemen, P. Ormos, J. Glückstad, Wave-guided optical waveguides, Opt. Express. 20 (2012) 2004–14. http://www.ncbi.nlm.nih.gov/pubmed/22330441.

[25] D. Palima, A.R. Bańas, G. Vizsnyiczai, L. Kelemen, T. Aabo, P. Ormos, J. Glückstad, Optical forces through guided light deflections., Opt. Express. 21 (2013) 581–93. http://www.ncbi.nlm.nih.gov/pubmed/23388951.

[26] M. Villangca, D.Z. Palima, A. Banas, J. Glückstad, Light-driven micro-tool equipped with a syringe function, Light Sci. Appl. 5 (2016).

[27] J.A. Hoffnagle, C.M. Jefferson, Design and performance of a refractive optical system that converts a Gaussian to a flattop beam., Appl. Opt. 39 (2000) 5488–99. http://www.ncbi.nlm.nih.gov/pubmed/18354545.

[28] W.B. Veldkamp, Laser beam profile shaping with interlaced binary diffraction gratings., Appl. Opt. 21 (1982) 3209–12. http://www.ncbi.nlm.nih.gov/pubmed/20396205.

[29] M.R. Wang, Analysis and optimization on single-zone binary flat-top beam shaper, Opt. Eng. 42 (2003) 3106. doi:10.1117/1.1617310.

[30] S.K. Case, P.R. Haugen, O.J. Lřkberg, Multifacet holographic optical elements for wave front transformations., Appl. Opt. 20 (1981) 2670–5. http://www.ncbi.nlm.nih.gov/pubmed/20333016.

[31] I. Gur, D. Mendlovic, Diffraction limited domain flat-top generator, (1998) 237–248.

[32] A.W. Lohmann, D.P. Paris, Binary fraunhofer holograms, generated by computer., Appl. Opt. 6 (1967) 1739–48. http://www.ncbi.nlm.nih.gov/pubmed/20062296.

[33] W.H. Lee, Sampled fourier transform hologram generated by computer, Appl. Opt. 9 (1970) 639–43. http://www.ncbi.nlm.nih.gov/pubmed/20076253.

[34] T.R.M. Sales, R.P.C. Photonics, C. Road, R. Ny, Structured Microlens Arrays for Beam Shaping, in: Proc. SPIE, 2003: pp. 109–120.

[35] C. Kopp, L. Ravel, P. Meyrueis, Efficient beamshaper homogenizer design combining diffractive optical elements, microlens array and random phase plate, J. Opt. A Pure Appl. Opt. 1 (1999) 398–403. doi:10.1088/1464-4258/1/3/310.

[36] R. Voelkel, K.J. Weible, Laser beam homogenizing: limitations and constraints, in: A. Duparré, R. Geyl (Eds.), Proc. SPIE, 2008: p. 71020J–71020J–12. doi:10.1117/12.799400.

[37] D. Gabor, others, A new microscopic principle, Nature. 161 (1948) 777–778.

[38] J.W. Cooley, J.W. Tukey, An algorithm for the machine calculation of complex Fourier series, Math. Comput. 19 (1965) 297–301.

[39] D. Palima, V.R. Daria, Holographic projection of arbitrary light patterns with a suppressed zero-order beam, Appl. Opt. 46 (2007) 4197–201. http://www.ncbi.nlm.nih.gov/pubmed/17579674.

[40] P. Korda, G.C. Spalding, E.R. Dufresne, D.G. Grier, Nanofabrication with holographic optical tweezers, Rev. Sci. Instrum. 73 (2002) 1956. doi:10.1063/1.1455136.

[41] I. Moreno, J. Campos, C. Goreck, M.J. Yzuel, Effects of amplitude and phase mismatching errors in the generation of a kinoform for pattern recognition, Jpn. J. Appl. Phys. 34 (n.d.) 6423–6432. http://cat.inist.fr/?aModele=afficheN&cpsidt=2937686 (accessed July 4, 2013).

[42] R.W. Gerchberg, W.O. Saxton, A practical algorithm for the determination of the phase from image and diffraction plane pictures, Optik (Stuttg). 35 (1972) 237–246.

[43] J.R. Fienup, Phase retrieval algorithms: a comparison, Appl. Opt. 21 (1982) 2758–69. http://www.ncbi.nlm.nih.gov/pubmed/20396114.

[44] N. Masuda, T. Ito, T. Tanaka, A. Shiraki, T. Sugie, Computer generated holography using a graphics processing unit, Opt. Express. 14 (2006) 603–8. http://www.ncbi.nlm.nih.gov/pubmed/19503377.

[45] J. Liesener, M. Reicherter, T. Haist, H.J. Tiziani, Multi-functional optical tweezers using computer-generated holograms, 185 (2000) 77–82.

[46] G. Sinclair, P. Jordan, J. Leach, M.J. Padgett, J. Cooper, Defining the trapping limits of holographical optical tweezers, J. Mod. Opt. 51 (2004) 409–414. doi:10.1080/09500340408235532.

[47] G. Thalhammer, R.W. Bowman, G.D. Love, M.J. Padgett, M. Ritsch-Marte, Speeding up liquid crystal SLMs using overdrive with phase change reduction., Opt. Express. 21 (2013) 1779–97. http://www.ncbi.nlm.nih.gov/pubmed/23389162.

[48] K. Dholakia, T. Čižmár, Shaping the future of manipulation, Nat. Photonics. 5 (2011) 335–342. doi:10.1038/nphoton.2011.80.

[49] L. Ge, M. Duelli, R. Cohn, Enumeration of illumination and scanning modes from real-time spatial light modulators., Opt. Express. 7 (2000) 403–16. http://www.ncbi.nlm.nih.gov/pubmed/19407892.

[50] T. Matsuoka, M. Nishi, M. Sakakura, K. Miura, K. Hirao, D. Palima, S. Tauro, A. Bańas, J. Glückstad, Functionalized 2PP structures for the BioPhotonics Workstation, in: D.L. Andrews, E.J. Galvez, J. Glückstad (Eds.), Proc. SPIE, 2011: p. 79500Q. doi:10.1117/12.877189.

[51] J. Glückstad, D. Palima, Generalized Phase Contrast: Applications in Optics and Photonics, Springer Series in Optical Sciences, 2009.
[52] F. Zernike, How I Discovered Phase Contrast, Science. 121 (1955) 345–349.
[53] D. Palima, J. Glückstad, Diffractive generalized phase contrast for adaptive phase imaging and optical security., Opt. Express. 20 (2012) 1370–7. http://www.ncbi.nlm.nih.gov/pubmed/22274481.
[54] D. Palima, A. Banas, M. Villangca, J. Glückstad, GPC and quantitative phase imaging, in: Proc. SPIE, 2016.
[55] V.R. Daria, P.J. Rodrigo, S. Sinzinger, J. Glückstad, Phase-only optical decryption in a planar integrated micro-optics system, Opt. Eng. 43 (2004) 2223–2227.
[56] J.G. Lee, B.J. McIlvain, C.J. Lobb, W.T. Hill, Analogs of basic electronic circuit elements in a free-space atom chip., Sci. Rep. 3 (2013) 1034. doi:10.1038/srep01034.
[57] J. Glückstad, Phase contrast image synthesis, Opt. Commun. 130 (1996) 225–230. doi:http://dx.doi.org/10.1016/0030-4018(96)00339-2.
[58] J. Glückstad, L. Lading, H. Toyoda, T. Hara, Lossless light projection., Opt. Lett. 22 (1997) 1373–1375. http://www.ncbi.nlm.nih.gov/pubmed/18188241.
[59] P.J. Rodrigo, V.R. Daria, J. Glückstad, Dynamically reconfigurable optical lattices, Opt. Express. 13 (2005) 1384–1394. doi:10.1364/OPEX.13.001384.
[60] C.A. Alonzo, P.J. Rodrigo, J. Glückstad, Photon-efficient grey-level image projection by the generalized phase contrast method, New J. Phys. 9 (2007) 132–132. doi:10.1088/1367-2630/9/5/132.
[61] J. Glückstad, D. Palima, P.J. Rodrigo, C.A. Alonzo, Laser projection using generalized phase contrast, Opt. Lett. 32 (2007) 3281–3283. doi:10.1364/OL.32.003281.
[62] D. Palima, C.A. Alonzo, P.J. Rodrigo, J. Glückstad, Generalized phase contrast matched to Gaussian illumination, Opt. Express. 15 (2007) 11971–7. http://www.ncbi.nlm.nih.gov/pubmed/19547560.
[63] A. Bańas, D. Palima, M. Villangca, T. Aabo, J. Glückstad, GPC light shaper for speckle-free one- and two- photon contiguous pattern excitation, Opt. Express. 7102 (2014) 5299–5310. doi:10.1364/OE.22.005299.
[64] A. Bańas, O. Kopylov, M. Villangca, D. Palima, J. Glückstad, GPC Light Shaper: static and dynamic experimental demonstrations, Opt. Express. (2014). doi:10.1364/OE.22.023759.
[65] S. Tauro, A. Bańas, D. Palima, J. Glückstad, Experimental demonstration of Generalized Phase Contrast based Gaussian beam-shaper., Opt. Express. 19 (2011) 7106–11. http://www.ncbi.nlm.nih.gov/pubmed/21503023.
[66] J. Glückstad, P.C. Mogensen, Optimal phase contrast in common-path interferometry., Appl. Opt. 40 (2001) 268–82. http://www.ncbi.nlm.nih.gov/pubmed/18357000.
[67] S. Tauro, A. Bańas, D. Palima, J. Glückstad, Experimental demonstration of Generalized Phase Contrast based Gaussian beam-shaper, Opt. Express. 19 (2011) 7106–11. http://www.ncbi.nlm.nih.gov/pubmed/21503023.
[68] D. Palima, J. Glückstad, Multi-wavelength spatial light shaping using generalized phase contrast, Opt. Express. 16 (2008) 1331–42. http://www.ncbi.nlm.nih.gov/pubmed/18542205.
[69] O. Kopylov, A. Bańas, M. Villangca, D. Palima, J. Glückstad, GPC light shaping a supercontinuum source, Optics Express 23 (2015) 1894–1905. doi:10.1364/OE.23.00184.
[70] Y. Tanaka, S. Tsutsui, M. Ishikawa, H. Kitajima, Hybrid optical tweezers for dynamic micro-bead arrays., Opt. Express. 19 (2011) 15445–51. http://www.ncbi.nlm.nih.gov/pubmed/21934908.
[71] S. Tauro, A. Bańas, D. Palima, J. Glückstad, Dynamic axial stabilization of counter-propagating beam-traps with feedback control, Opt. Express. 18 (2010) 18217–22. http://www.ncbi.nlm.nih.gov/pubmed/20721211.
[72] H.-U. Ulriksen, J. Thogersen, S. Keiding, I. Perch-Nielsen, J. Dam, D. Palima, H. Stapelfeldt, J. Glückstad, Independent trapping, manipulation and characterization by an all-optical biophotonics workstation, J. Eur. Opt. Soc. Rapid Publ. 3 (2008). doi:10.2971/jeos.2008.08034.
[73] M. Villangca, A. Bańas, D. Palima, J. Glückstad, Dynamic diffraction-limited light-coupling of 3D-maneuvered waveguided optical waveguides, Opt. Express. 22 (2014) 17880–17889. doi:10.1364/OE.22.017880.
[74] A. Bańas, T. Aabo, D. Palima, J. Glückstad, Matched filtering Generalized Phase Contrast using binary phase for dynamic spot- and line patterns in biophotonics and structured lighting, Optics Express 21 (2013) 1849–1856. doi:10.1002/jbio.201100101.D.
[75] A. Bańas, J. Glückstad, Holo-GPC: Holographic Generalized Phase Contrast, Opt. Commun. 392 (2017) 190–195. doi:http://dx.doi.org/10.1016/j.optcom.2017.01.036.
[76] D. Palima, C.A. Alonzo, P.J. Rodrigo, J. Glückstad, Generalized phase contrast matched to Gaussian illumination, Opt. Express. 15 (2007) 11971–11977. http://www.ncbi.nlm.nih.gov/pubmed/19547560.
[77] A.R. Bańas, M.J. Villangca, D. Palima, J. Glückstad, Dark GPC, in: SPIE OPTO, 2016: p. 97640H–97640H.
[78] F. Kenny, F.S. Choi, J. Glückstad, M.J. Booth, Adaptive optimisation of a generalised phase contrast beam shaping system, Opt. Commun. 342 (2015) 109–114. doi:10.1016/j.optcom.2014.12.059.
[79] R. Porras-Aguilar, K. Falaggis, J.C. Ramirez-San-Juan, R. Ramos-Garcia, Self-calibrating common-path interferometry, Opt. Express. 23 (2015) 3327. doi:10.1364/OE.23.003327.
[80] M.J. Villangca, A.R. Bańas, D. Palima, J. Glückstad, Dark GPC: extended nodal beam areas from binary-only phase, Opt. Eng. 55 (2016) 125102. doi:10.1117/1.OE.55.12.125102.
[81] G.J. Ruane, G.A. Swartzlander, S. Slussarenko, L. Marrucci, M.R. Dennis, Nodal areas in coherent beams, Optica. 2 (2015) 147–150. doi:10.1364/OPTICA.2.000147.
[82] V. Daria, J. Glückstad, P.C. Mogensen, R.L. Eriksen, S. Sinzinger, Implementing the generalized phase-contrast method in a planar-integrated micro-optics platform., Opt. Lett. 27 (2002) 945–7. http://www.ncbi.nlm.nih.gov/pubmed/18026332.
[83] D. Palima, J. Glückstad, Gaussian to uniform intensity shaper based on generalized phase contrast, Opt. Express. 16 (2008) 1507–16. http://www.ncbi.nlm.nih.gov/pubmed/18542226.
[84] M. Villangca, A. Bańas, O. Kopylov, D. Palima, J. Glückstad, Optimal illumination of phase-only diffractive element using GPC light shaper, in: Proc. SPIE, 2015: pp. 9379–24.
[85] M. Villangca, A. Bańas, D. Palima, J. Glückstad, GPC-enhanced read-out of holograms, Opt. Commun. 351 (2015) 121–127. doi:http://dx.doi.org/10.1016/j.optcom.2015.04.057.
[86] H.O. Bartelt, Applications of the tandem component: an element with optimum light efficiency., Appl. Opt. 24 (1985) 3811. http:

//www.ncbi.nlm.nih.gov/pubmed/18224124.

[87] H.O. Bartelt, Computer-generated holographic component with optimum light efficiency., Appl. Opt. 23 (1984) 1499. http://www.ncbi.nlm.nih.gov/pubmed/18224124.

[88] A. Jesacher, C. Maurer, A. Schwaighofer, S. Bernet, M. Ritsch-Marte, Near-perfect hologram reconstruction with a spatial light modulator., Opt. Express. 16 (2008) 2597–603. http://www.ncbi.nlm.nih.gov/pubmed/18542342.

[89] M.A. Go, P.-F. Ng, H. a Bachor, V.R. Daria, Optimal complex field holographic projection., Opt. Lett. 36 (2011) 3073–5. http://www.ncbi.nlm.nih.gov/pubmed/21847164.

[90] D. Palima, J. Glückstad, Comparison of generalized phase contrast and computer generated holography for laser image projection, Opt. Express. 16 (2008) 5338–5349. http://www.ncbi.nlm.nih.gov/pubmed/18542636.

[91] A. Bańas, D. Palima, J. Glückstad, Matched-filtering generalized phase contrast using LCoS pico-projectors for beam-forming., Opt. Express. 20 (2012) 9705–9712. http://www.ncbi.nlm.nih.gov/pubmed/22535062.

[92] A. Martínez, N. Beaudoin, I. Moreno, M.D.M. Sánchez-López, P. Velásquez, Optimization of the contrast ratio of a ferroelectric liquid crystal optical modulator, J. Opt. A Pure Appl. Opt. 8 (2006) 1013–1018. doi:10.1088/1464-4258/8/11/013.

[93] Syndiant SYL2043 Product Brief, (n.d.). http://syndiant.com/pdfs/SYL2043_ProductBrief.pdf.

[94] J. Yamamoto, T. Iwai, Spatial Stability of Particles Trapped by Time-Division Optical Tweezers, Int. J. Optomechatronics. 3 (2009) 253–263. doi:10.1080/15599610903391168.

[95] I. Perch-Nielsen, D. Palima, J. Dam, J. Glückstad, Parallel particle identification and separation for active optical sorting, J. Opt. A Pure Appl. Opt. 11 (2009) 34013. doi:10.1088/1464-4258/11/3/034013.

[96] A. Bańas, T. Aabo, D. Palima, J. Glückstad, Matched filtering Generalized Phase Contrast using binary phase for dynamic spot- and line patterns in biophotonics and structured lighting, Opt. Express. 21 (2013) 388–394. doi:10.1002/jbio.201100101.D.

[97] A. Bańas, D. Palima, J. Glückstad, Matched-filtering generalized phase contrast using LCoS pico-projectors for beam-forming., Opt. Express. 20 (2012) 9705–12. http://www.ncbi.nlm.nih.gov/pubmed/24258701.

[98] H. Dammann, E. Klotz, Coherent Optical Generation and Inspection of Two-dimensional Periodic Structures, Opt. Acta Int. J. Opt. 24 (1977) 505–515. doi:10.1080/713819570.

[99] M. Zenou, M. Reznikov, M. Manevich, J. Varshal, Y. Reznikov, Z. Kotler, Adaptive beam shaper based on a single liquid crystal cell, Opt. Commun. 290 (2013) 115–117. doi:10.1016/j.optcom.2012.10.018.